El Niño Southern Oscillation influence on the Asian summer monsoon anticyclone

Xiaolu Yan[1,2], Paul Konopka[1], Felix Ploeger[1], Mengchu Tao[1], Rolf Müller[1], Jianchun Bian[2,3], and Martin Riese[1]

[1]Forschungszentrum Jülich (IEK-7: Stratosphere), Jülich, Germany
[2]Key Laboratory of Middle Atmosphere and Global Environment Observation (LAGEO), Institute of Atmospheric Physics, Chinese Academy of Sciences, Beijing, China
[3]College of Earth Science, University of Chinese Academy of Sciences, Beijing, China

Correspondence to: Xiaolu Yan (x.yan@fz-juelich.de)

Abstract. We analyze the influence of the El Niño Southern Oscillation (ENSO) on the atmospheric circulation and the mean ozone distribution in the tropical and sub-tropical UTLS region. In particular, we focus on the impact of ENSO on the onset of the Asian summer monsoon (ASM) anticyclone. Using the Multivariate ENSO Index, we define climatologies (composites) of atmospheric circulation and composition in the months following El Niño and La Niña (boreal) winters and investigate how

5   ENSO-related flow anomalies propagate into spring and summer. To quantify differences in the divergent and non-divergent part of the flow, the velocity potential (VP) and the stream function (SF) respectively, are calculated from the ERA-Interim reanalysis around the tropical tropopause (potential temperature level θ=380 K). While VP quantifies the well-known ENSO anomalies of the Walker circulation, SF can be used to study the impact of ENSO on the formation of the ASM anticyclone which turns out to be slightly weaker after El Niño than after La Niña winters. In addition, stratospheric intrusions around

10   the eastern flank of the anticyclone into the Tropical Tropopause Layer (TTL) are weaker in the months after strong El Niño events due to more zonally symmetric subtropical jets than after La Niña winters. By using satellite (MLS), in-situ (SHADOZ) observations and model simulations (CLaMS) of ozone, we discuss ENSO-induced differences around the tropical tropopause. Ozone composites show more zonally symmetric features with less in-mixed ozone from the stratosphere into the TTL during and after strong El Niño events and even during the formation of the ASM anticyclone. The difference between El Niño and

15   La Niña composites becomes statistically insignificant in late summer.

1   Introduction

El Niño and La Niña are opposite phases of the El Niño Southern Oscillation (ENSO) which originates from the coupled interaction between the tropical Pacific and the overlying atmosphere (e.g., Bjerknes, 1929; Wang and Picaut, 2004). ENSO is widely recognized as a dominant mode of the Earth's climate variability (McPhaden et al., 2006). In the troposphere, ENSO

20   manifests in the anomalies of the zonal distribution of convection which are triggered by a positive (El Niño) and negative (La Niña) sea surface temperature (SST) anomaly in the central and eastern Pacific (Philander et al., 1989). The SST anomalies

Atmospheric
Chemistry
and Physics
Discussions

typically peak during the Northern Hemisphere (NH) winter time (hereafter, seasons refer to the NH), but prolonged events may last for months or years (Moron and Gouirand, 2003; McPhaden, 2015).

Strong El Niño events disrupt the Walker circulation and lead to its breakdown during the warm ocean phases (Wang et al., 2002). Strong El Niño events also propagate upwards above the tropopause by accelerating the Brewer Dobson circulation

5 (BDC) and moistening the stratosphere (Scaife et al., 2003; Randel et al., 2009; Calvo et al., 2010). Using satellite observations and model simulations of water vapour and mean age of air, Konopka et al. (2016) have recently shown that wet (dry) and young (old) tape-recorder anomalies propagate upwards in the tropical lower stratosphere in the months following El Niño (La Niña). They found that these anomalies are around $+0.3$ (-0.2) ppmv and -4 $(+4)$ months for water vapour and age of air, respectively.

10 The Asian summer monsoon (ASM) anticyclone is a dominant feature of the circulation in the upper troposphere lower stratosphere (UTLS) during summer (Dethof et al., 1999; Randel and Park, 2006; Park et al., 2007). This nearly stationary anticyclone extends well into the lower stratosphere up to about 18 km (or $\theta =420$ K) and effectively isolates the air masses of tropospheric origin inside from the much older, mainly stratospheric air outside this anticyclone (Park et al., 2008; Ploeger et al., 2015). This anticyclone has been repeatedly identified as a key pathway for stratosphere-troposphere exchange (STE) in sum-

15 mer and fall, both quasi-isentropically into the lowermost stratosphere and into the upper branch of the Brewer Dobson circulation, especially for water vapour and pollutants entering the global stratosphere (Bannister et al., 2004; Fueglistaler et al., 2005; Fu et al., 2006; Randel et al., 2010; Wright et al., 2011; Vogel et al., 2016; Ploeger et al., 2017).

Generally, an enhanced isentropic STE between the extratropics and tropics is caused by the monsoon systems, in particular by the ASM during NH summer (Dunkerton, 1995; Chen, 1995). Haynes and Shuckburgh (2000) showed that, indeed, the

20 subtropical jet acting as a transport barrier between the extratropics and tropics weakens during NH summer. Consequently, enhanced isentropic transport occurs in both directions, out of the tropics and from the extratropics into the tropics (termed inmixing, in the following). Related stratospheric signatures can be found in the Tropical Tropopause Layer (TTL) as diagnosed from the NASA's Aura Microwave Limb Sounder (MLS) observations of HCl and ozone (Santee et al., 2011, 2017). This inmixed ozone contributes to more than half of the annual cycle of ozone in the upper part of the TTL (Konopka et al., 2010;

25 Ploeger et al., 2012). Enhanced quasi-isentropic transport from the tropics to the midlatitude lowermost stratosphere driven by the ASM is also clearly observed both for tracers and water vapor (Ploeger et al., 2013; Müller et al., 2016; Vogel et al., 2016; Rolf et al., 2017)
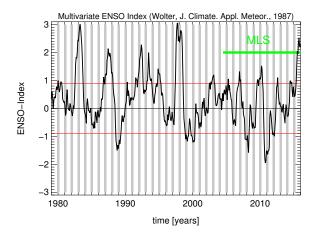
A regionally-resolved view on the processes coupling ENSO with the stratosphere, mainly during the winter and spring, has been adopted in several previous studies (Krüger et al., 2008; Liess and Geller, 2012; Garfinkel et al., 2013; Konopka et al.,

30 2016). However, there are only few publications investigating the impact of ENSO on the ASM anticyclone and on the related STE (Ju and Slingo, 1995; Kawamura, 1998; Wang et al., 2013). This is in contrast with a large number of investigations connecting ENSO with the tropospheric variability of the ASM like weather patterns or precipitation, which have a long tradition starting with the pioneering studies of Walker (1923) and Bjerknes (1969).

In this study, we investigate how the ENSO winter signal propagates into the following seasons. In particular, we charac-

35 terize the impact of ENSO on the upper branches of the Walker and Hadley circulation in the UTLS. We focus on the ASM

Atmospheric
Chemistry
and Physics
Discussions

Figure 1. Multivariate ENSO Index (MEI) from the NOAA Climate Diagnostic Center, http://www.esrl.noaa.gov/psd/enso/mei, (Wolter, 1987). The red lines denote the threshold values (±0.9) defining the El Niño (positive) and La Niña (negative) composites as used in this paper. Gray shading shows winter seasons (December-February, DJF).

anticyclone, its strength as well as its efficiency for in-mixing of stratospheric ozone into the TTL. We investigate how long ENSO related statistically relevant differences can be diagnosed in the TTL both in the meteorological reanalysis as well as in long-term satellite and in-situ ozone observations. Section 2 discusses data and methods for our analysis. Section 3 describes the seasonal propagation of ENSO anomalies. Section 4 quantifies the influence of ENSO anomalies on the seasonality of
5   ozone in the TTL. Finally, section 5 provides the summary and conclusions.

2   Data and methods

There are several indices to indicate the phase of ENSO, and they are highly correlated (Pumphrey et al., 2017). Here, the Multivariate ENSO Index (MEI, Fig. 1) from the NOAA Climate Diagnostic Center, http://www.esrl.noaa.gov/psd/enso/mei, is used to quantify the ENSO variability(Wolter, 1987). MEI is calculated based on sea surface pressure, zonal and meridional
10 components of the surface wind, SST and total cloudiness fraction of the sky over the tropical Pacific. The two phases of ENSO typically show pronounced features in late fall, winter and early spring (Moron and Gouirand, 2003; McPhaden, 2015). Correspondingly, MEI shows peak value during this period. Negative and positive values of MEI quantify La Niña and El Niño events, respectively.

Hereafter, we define two winter composites (December-February, DJF) of ENSO events by the condition MEI< -0.9 for La
15 Niña and MEI>0.9 for El Niño (red lines in Fig. 1) as discussed in Konopka et al. (2016). The winter months defining these two composites (17 for La Niña and 28 for El Niño) are listed in Table 1. The QBO phase during the considered months is also listed (https://www.esrl.noaa.gov/psd/data/correlation/qbo.data) and shows that our composites are only weakly biased by the westerly phase.

3

Atmospheric
Chemistry
and Physics
Discussions

	La Niña			El Niño	
Year	Months	QBO	Year	Months	QBO
88/89	DJF	W	79/80	D	E
98/99	DJF	E	82/83	DJF	W
99/00	DJF	W	86/87	DJF	E
07/08	DJF	E	87/88	DJ	W
10/11	DJF	W	91/92	DJF	E
11/12	DJ	W/E	92/93	F	W
			94/95	DJF	E/W
			97/98	DJF	W
			02/03	DJF	W
			06/07	DJ	W
			09/10	DJF	E
			15/16	D	W

Table 1. List of all relevant La Niña and El Niño winter months during the period of 1979-2015. In total there are 17 and 28 months for the La Niña and El Niño composites, respectively, which are listed above (D/J/F for December, January and February). Within the La Niña composite there are 7 months in the easterly phase (E) and 10 months in the westerly phase (W) of the QBO (defined by 30 day smoothed equatorial wind at 50 hPa). For El Niño composites 11 months are in the easterly phase and 17 months in the westerly phase.

To study the effect of strong ENSO winters on the UTLS in the following months, we also consider climatologies of "shifted" composites for different seasons, e.g., DJF, JFM, FMA, MAM, AMJ, MJJ, and JJA). The mean value of a composite is defined from the averaged monthly means of its elements. We call two (La Niña and El Niño) composites statistically different when the significance Monte Carlo test for their difference is passed at a 95% confidence level after at least 1000 iteration steps.

5   To quantify ENSO anomalies in the climatological flow patterns, stream function (SF) ψ and velocity potential (VP) χ are calculated (Tanaka et al., 2004) using meteorological data from ERA-Interim reanalysis during 1979-2015 (Dee et al., 2011). According to the Helmholtz theorem, an arbitrary 2D horizontal flow $\mathbf{u} = (u, v)$ can be separated into a non-divergent (i.e. rotational) part $\mathbf{u_a}$ with $\nabla \cdot \mathbf{u_a} = 0$ and a divergent (i.e. irrotational) part $\mathbf{u_b}$ with $\nabla \times \mathbf{u_b} = 0$, i.e.,

$$\mathbf{u} = \mathbf{u_a} + \mathbf{u_b} = \mathbf{k} \times \nabla \psi + \nabla \chi, \tag{1}$$

10   where both parts can also be expressed in terms of the potentials ψ and χ. Here, $\mathbf{k}$ denotes the unit vector perpendicular to the considered 2D surface. SF and VP are scalar quantities which are easy to plot and widely applied in meteorology and oceanography to represent large scale flow fields (see e.g., Evans and Allan, 1992; Kunze et al., 2016). SF quantifies the position and strengths of the cyclones and anticyclones. Following Tanaka et al. (2004), we use VP to represent the Walker circulation and the zonal mean of VP to quantify the Hadley circulation. SF and VP will be divided into El Niño and La Niña

15   composites as described above for this study.

Atmospheric
Chemistry
and Physics
Discussions

To validate our diagnostic of the flow and understand the effect of ENSO on the atmospheric composition in the UTLS region, ozone distribution is used to represent the influence. MLS ozone data (version 4.2) and the Hilo (Hawaii) ozonesonde data from Southern Hemisphere ADditional OZonesondes (SHADOZ) (Thompson et al., 2007) are used (see http://croc.gsfc.nasa.gov/shadoz) as references. MLS measurements provide 8/6 months of data for the La Niña/El Niño composites from 2004 to 2015. Respec-
5   tively there are 14 and 11 months of data for the La Niña and El Niño composites from SHADOZ ozondesonde covering the pe-
riod 1998-2015. Chemical Lagrangian Model of the Stratosphere (CLaMS) simulations (McKenna et al., 2002; Konopka et al., 2004; Pommrich et al., 2014) driven by the ERA-Interim reanalysis are used to obtain robust statistical composites of ozone (with the same number of La Niña/El Niño months like for SF and VP). Outgoing long-wave radiation (OLR) monthly data from NOAA during 1979-2015 complete our analysis as a proxy for deep convection (see http://www.esrl.noaa.gov/psd/enso/mei).

10 ## 3 ENSO anomalies at the tropical tropopause from winter to summer

In this section, we use the composites of the stream function (SF) and the velocity potential (VP) introduced above to illustrate some ENSO-related differences in the mean flow properties around the tropical tropopause.

3.1 Cyclones and anticyclones

Seasonal variations of SF after strong La Niña and El Niño winters are shown in Fig. 2. Here, respective climatologies are
15 plotted at the potential temperature level θ=380 K, which roughly marks the tropopause in the tropics and separates the over-world in the extratropics from the lowermost stratosphere (Holton et al., 1995; Gettelman et al., 2011). The panels start from the winter (top, DJF) and end with the summer distribution (bottom, JJA).

Because the divergent part of the flow at θ=380 K is very small compared to the rotational part of the flow, isolines of SF approximate the climatological streamlines whereas strongest horizontal gradients of SF describe the highest flow velocities.
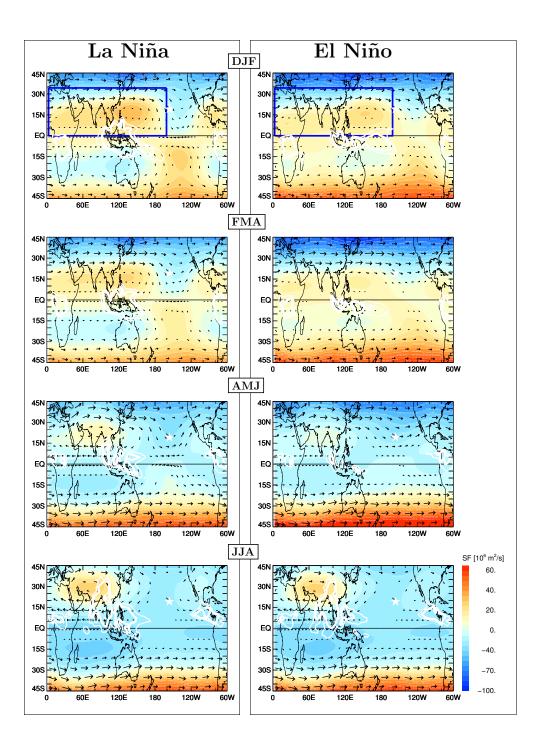20 The anticyclones are represented by its positive and negative values in NH and SH with highest and lowest values corresponding to their centers, respectively. During DJF, the flow in the tropical UTLS between 60° E and 120° W is dominated by two equatorially symmetric anticyclones resembling the well-known (symmetric) Matsuno-Gill solution with the heat source from convection located symmetrically over the equator (Matsuno, 1966; Gill, 1980; Highwood and Hoskins, 1998).

The climatological sources of heat can be approximated by the lowest values of the OLR using the same type of composites
25 like for SF (white contours in Fig. 2). Thus, following the symmetric Matsuno-Gill solution as a proxy, the relevant latent heat sources for the anticyclones originate mainly in western Pacific, especially during La Niña, and these sources are partially shifted to the east, during El Niño events.

Over the course of the following 6 months, as the ITCZ moves northwards, these two anticyclones shift to the north-west roughly following the position of convection (Highwood and Hoskins, 1998). The anticyclone in the NH intensifies, starting in
30 May and June, and forms the well-known Asian summer monsoon (ASM) anticyclone. In addition a weaker anticyclone in the Southern Hemisphere can also be diagnosed. Thus, the summer configuration resembles more a superposition of a symmetric and asymmetric Matsuno-Gill solution (Zhang and Krishnamurti, 2006).

Figure 2. Climatologies (composites) of the stream function (SF, in 10^6 m^2/s) at θ=380 K calculated from ERA-Interim (1979-2015) for months following La Niña (left) and El Niño (right) winter until summer (from top to bottom). The arrows represent the rotational horizontal wind. White isolines indicate the strong convection regions based on OLR (thick and thin lines represent 210 and 220 W/m^2 contours) data, respectively. Hereafter, the star in the figure marks the location of the SHADOZ station used in this study (Hilo, Hawaii).
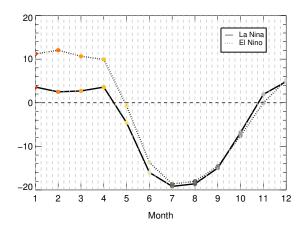
Figure 3. Mean wind over south-east Asia ([5° N, 20° N; 40° E, 120° E]) following La Niña and El Niño winters at θ=340 K.

Now we discuss the differences in the large-scale flow in the UTLS caused by the ENSO (i.e. differences between the left and the right column of Fig. 2). The most striking difference in DJF is a much weaker meridional disruption of the subtropical jets during El Niño than during La Niña winters, mainly in the NH subtropics between 170° E and 70° W. At the lower levels (not shown), such stratospheric intrusions coincide with regions of the so called "westerly ducts" which are much weaker during El Niño (Waugh and Polvani, 2000).

Furthermore, the equatorially symmetric anticyclones are more pronounced for the La Niña composites due to a stronger localized convection in the western Pacific. These differences are also present during FMA, become smaller during AMJ and disappear during JJA mainly because forcing of the summer dynamics, especially of the ASM, is only weakly related to the winter forcing.

The mean anticyclone in AMJ is similar to the beginning phase of ASM anticyclone after El Niño winters, while it is closer to the mature phase after La Niña winters. We use the transition of the upper-level (at 200 hPa) flow from westerly to easterly over south-east Asia [5° N, 20° N; 40° E, 120° E] to characterize the onset of the monsoon as used in Ju and Slingo (1995). It turns out that the onset of ASM after La Niña is about half month earlier than after El Niño (Fig. 3). The difference in SF between La Niña and El Niño composites lasts from winter (DJF) to early summer (AMJ) and becomes insignificant in summer (JJA).
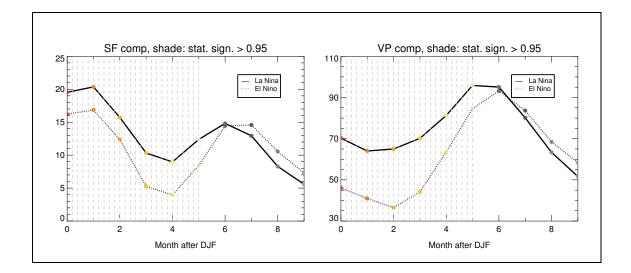
To prove the statistical significance of the ENSO anomalies in the SF composites, we compare their mean values averaged over a representative region shown as a blue rectangle in Figs. 2. The domain, defined as [0° N, 35° N; 0° E, 160° W], contains the NH anticyclone from winter to summer. The results are shown in the left panel of Fig. 4. The period with statistically different composites is grey hatched. Thus, the NH anticyclone in La Niña years is significantly stronger than in El Niño years within the first 5 months of the year, i.e. until MJJ. This statistical analysis indicates that the influence of ENSO on the anticyclone propagates from winter until early summer. The mean SF difference between La Niña and El Niño composites from winter to early summer is $\sim 6 \times 10^6 \, \text{m}^2/\text{s}$.

Figure 4. The average value of the stream function (left, in 10^6 m^2/s) in the domain of [0° N, 35° N; 0° E, 160° W] and velocity potential (right, in 10^5 m^2/s) in the domain of [20° S, 40° N; 90° E, 140° W] for La Niña (solid line) and El Niño (dot line) composites at θ=380 K. The dashed region denotes a period with statistically significant differences between the two composites.

3.2 Walker circulation

Complementary to SF, the divergent part of the horizontal flow can be described by the velocity potential VP and is shown in Fig. 5. Note that VP is by a factor of 10 smaller than SF, which is consistent with the fact that the non-divergent rather than divergent part dominates the flow at θ=380 K. Following Tanaka et al. (2004), the positive peak of VP indicates the intensity

5 of the Walker circulation and the zonal mean of VP ($\overline{\text{VP}}$) quantifies the Hadley circulation (see below). The positive values of VP represent divergence or, using the continuity equation, the strength of upwelling, while the negative values are related to convergence or downwelling. In this way, the upper branch of the Walker circulation can be diagnosed in Fig. 5. The intensities of the Walker circulation are similar to the results from Tanaka et al. (2004).

The positive peak values of VP lie in the western and central tropical Pacific for La Niña and El Niño DJF climatologies,

10 respectively. They correspond to the locations of rising motion. The mean upwelling (downwelling) activity in La Niña winters is much stronger than in El Niño winters in agreement with the well-known weakening of the Walker circulation after El Niño events (Wang et al., 2002). In spring (FMA) these differences become smaller than in winter for both composites. At the beginning of summer (AMJ), the centers of the divergence start to shift from the tropics to the extratropics and the differences become even smaller. In JJA, these centers reach the China Sea. The strength and position of the convergence/divergence

15 centers in the La Niña composite is comparable with that of El Niño.

Similarly as for SF, the statistical significance of the ENSO anomalies in the VP composites is diagnosed in the right panel of Fig. 4. The mean values over the blue rectangle in Fig. 5, defined as [20° S, 40° N; 90° E, 140° W], are calculated. The domain quantifies the average upwelling of the Walker circulation. The divergence in the La Niña composite is significantly
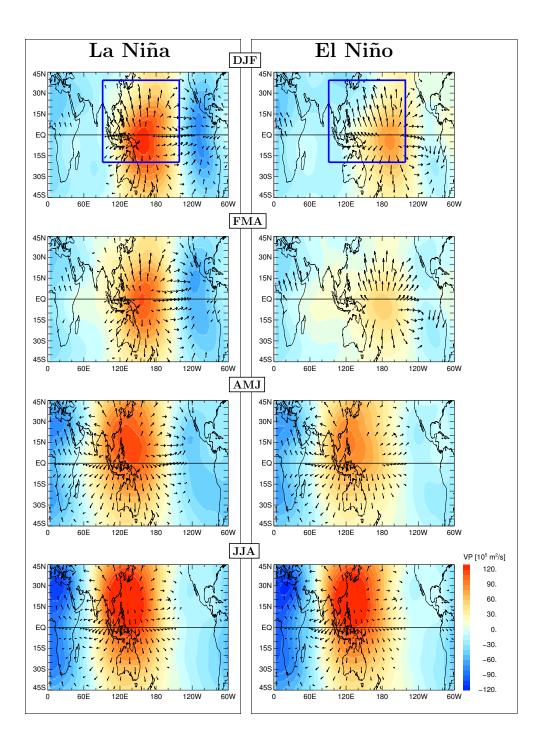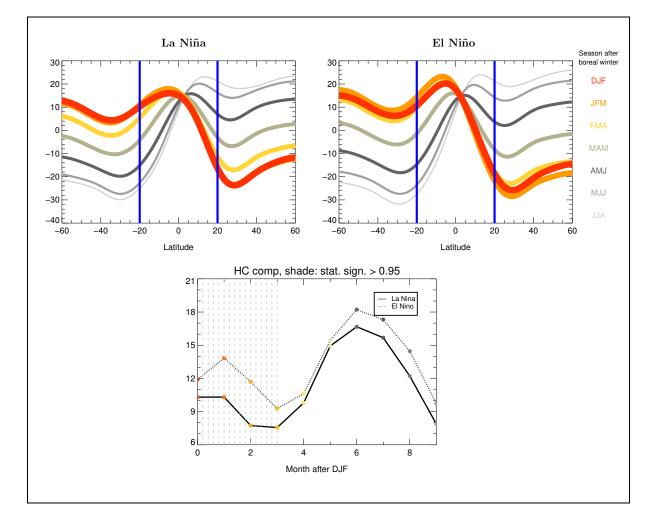
Figure 5. Same as Fig. 2 but for the velocity potential VP (in 10^5 m^2/s) at θ=380 K with arrows denoting the divergent part of the horizontal wind.

Figure 6. Zonal mean of the velocity potential at θ=360 K defining the Hadley circulation and calculated for La Niña and El Niño composites (top). The average intensity of Hadley circulation calculated for the domain of [$20°$ S, $20°$ N] (bottom).

higher than in the El Niño composite within the first 5 months of the year. The mean VP difference between La Niña and El Niño composites from winter to early summer is $\sim 22 \times 10^5 \, \mathrm{m^2/s}$.

3.3 Hadley circulation

The zonal mean of VP is used to represent the Hadley circulation (Fig. 6, top). Note that the values of VP are by more than three
5   times larger than $\overline{\mathrm{VP}}$. In winter, the zonal mean of VP is positive in SH and negative in NH. The positive peaks represent the locations of rising air and correspond to the inter-tropical convergence zone (ITCZ). The negative peaks represent the locations of sinking air. The rising and sinking motions form the mean meridional Hadley circulation. This circulation is weaker after La Niña than after El Niño with decreasing ENSO differences from DJF to JJA.

Atmospheric
Chemistry
and Physics
Discussions

The latitudes of positive peaks show that the rising motion is shifted southwards after El Niño winters compared to La Niña winters. Correspondingly, the ITCZ is located around 4° S and 6° S for the La Niña and El Niño composites, respectively. To check the statistical significance of such differences, the average rising intensity of the Hadley circulation in tropics (from 20° S to 20° N) is calculated (Fig. 6, bottom). The values after El Niño winters are stronger than after La Niña winters, especially during DJF and MAM. The mean difference is about 2×10^5 m²/s, and becomes insignificant starting from April.

4   Impacts on ozone distribution

So far we have investigated the influence of ENSO anomalies on the atmospheric circulation, especially on the mean horizontal flow quantified in term of the stream function SF (Fig. 2) and velocity potential VP (Fig. 5). Such changes of the atmospheric circulation will also affect the distribution of atmospheric constituents (Randel et al., 2009; Ziemke et al., 2015). Ozone is a sensitive indicator of transport properties in the UTLS region due to its strong vertical and horizontal gradients and its relatively long chemical lifetime. Furthermore, in the sub- and extratropics around the subtropical jet, the ozone distribution is mainly determined by transport rather than by chemistry. In this section, we quantify the impact of ENSO anomalies on the mean ozone distribution based on MLS satellite data, CLaMS simulations and SHADOZ ozonesonde data.

Particularly, the influence of ENSO on the isentropic in-mixing of high stratospheric ozone values into the tropical TTL is investigated (Konopka et al., 2010). In the following, the ozone isoline at tropopause is used to quantify the effect of isentropic in-mixing at 380 K potential temperature. Thouret et al. (2006) estimated the monthly mean climatological ozone concentration at the tropopause based on MOZAIC measurements. They found a maximum value in May (120 ppbv) and a minimum value in November (65 ppbv). Here, the isoline of 120 ppbv is used as the ozone boundary for CLaMS composites to obtain a conservative estimate of stratospheric influence. MLS ozone is high biased by ∼40% at 100 hPa in the tropics (Jiang et al., 2007) and even by ∼70% inside the ASM anticyclone (Yan et al., 2016). The precision of MLS ozone at tropopause is about 40 ppbv (Livesey et al., 2017). Therefore, the isoline of 185 ppbv is used as a proxy at the tropopause in the MLS composites.
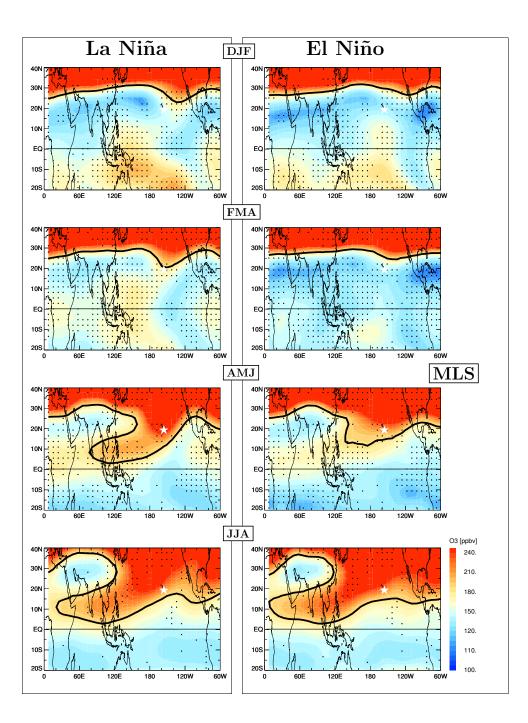
4.1   MLS composites

Fig. 7 shows MLS ozone mixing ratio distributions at θ=380 K from winter to summer after La Niña and El Niño winters. The ozone isoline at tropopause is represented by the black solid line. During DJF and FMA, the El Niño composite is more zonally symmetric compared to La Niña. This is consistent with the zonally symmetric pattern of the SF in El Niño winters as discussed in the last section. The region of enhanced in-mixing can be recognized as a tongue of high ozone which emerges around 120° W, 30° N during DJF and is shifted in the following months to the west until the ASM anticyclone forms.

During AMJ, this feature of in-mixing is much more pronounced for the La Niña than for the El Niño composite. This may be related to the differences in the phase of the ASM anticyclone between La Niña and El Niño shown in Fig. 2. The mean anticyclone in AMJ show similar feature to the ASM anticyclone in the beginning phase after El Niño, while ASM anticyclone after La Niña is close to the mature phase during this period. The largest pattern difference between La Niña and El Niño composites occurs during this period. Ozone in-mixing anomalies seem to be delayed compared to the distribution of SF.
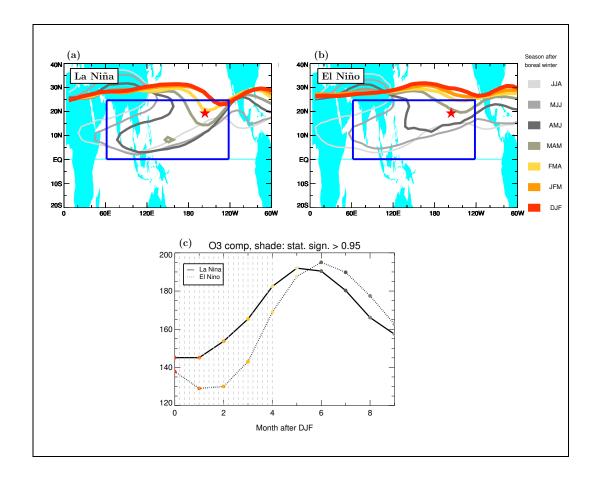
Atmospheric
Chemistry
and Physics
Discussions

Figure 7. Seasonal ozone climatology derived from MLS observations (2004-2015, version 4.2) at θ=380 K for La Niña and El Niño composites from winter to summer months (from top to bottom). The statistically significant regions are marked by the black dots. The black isolines represent ozone at tropopause with 185 ppbv (see text).

Figure 8. Top: Isolines of MLS ozone (185 ppbv, black lines in Fig. 7) at θ=380 K for different seasons following La Niña (a) and El Niño (b) winters (from DJF (red) to JJA (grey)). Bottom: The mean concentration of ozone from the blue domain in the top panel ([0° N, 25° N; 60° E, 120° W]) marking the region of strongest ENSO-related differences in in-mixing (c).

The black dots in Fig. 7 provide the information about regions with statistically significant differences between La Niña and El Niño composites. Thus, such differences mainly exist in the regions of strong in-mixing described above. During the mature phase of ASM anticyclone (JJA), the significantly different regions between La Niña and El Niño composites slightly decrease. Ozone values in the center of the ASM anticyclone are lower after La Niña than after El Niño winters which is consistent with

5   the similar differences in SF and VP (c.f. Fig. 2 and Fig. 5).

The isolines of the ozone at the tropopause are combined together in Fig. 8 (a) and (b) to illustrate the pattern of the seasonality of the ENSO-related differences in in-mixing. To quantify such differences, the mean concentration inside the blue domain [0° N, 25° N; 60° E, 120° W] is calculated and shown in the bottom panel of Fig. 8 (c). The dashed lines represent the significantly different seasons between La Niña and El Niño composites, which are from DJF to AMJ. The average results

10   inside the in-mixing region attest that ozone concentration after El Niño is about 16 ppbv lower than after La Niña from winter (DJF) to early summer (AMJ). The difference manifests the influence of stronger Hadley/BD-circulation and weaker
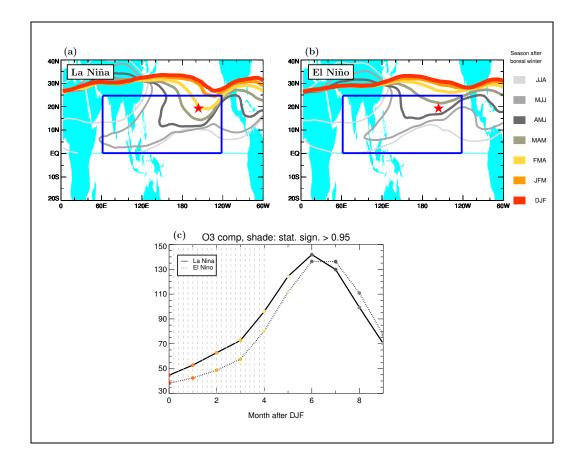
Figure 9. Same as Fig. 8 but for CLaMS ozone with the isoline value of 120 ppbv.

in-mixing after El Niño than after La Niña (Randel et al., 2009; Calvo et al., 2010; Konopka et al., 2016) on ozone horizontal distribution around tropopause. Starting from summer, the difference of ozone distribution between El Niño and La Niña becomes insignificant.

4.2 In-mixing from CLaMS

5 As discussed in Konopka et al. (2016, Figure 5), CLaMS reproduces fairly well the ENSO anomalies in ozone observed by MLS. However, the MLS composites cover only 11 years with few strong El Niño/La Niña events. Using CLaMS ozone, we are able to extend our period to 37 years from 1979 to 2015 and obtain more statistically robust results.

Fig. 9 (top) shows the same type of distribution like Fig. 8 but for 37-years of CLaMS ozone simulations. The isolines represent the ozone at the tropopause with 120 ppbv. They are used to characterize the ozone distribution after ENSO. The

10 ozone concentration from CLaMS simulations are about 50 ppbv lower than MLS measurements at $\theta=380$ K for both La Niña and El Niño during all seasons partially because of the zero ozone boundary condition at the ground, but they show similar patterns to MLS ozone. The CLaMS ozone distributions also show in-mixing activity over eastern and central Pacific

in subsequent months following La Niña winters, with more zonally symmetric features during months following El Niño. The signatures of in-mixing over the tropical Pacific become much stronger after the onset of the ASM anticyclone (AMJ) for both composites. The ozone intrusion from high latitude into the TTL is deeper following La Niña than following El Niño. The differences disappear in JJA.

5   The largest difference between the ENSO composites exists around the eastern flank of the ASM anticyclone. To quantify this difference from CLaMS simulations, the mean concentration in the blue domain (same as for MLS) is calculated. The results are shown in Fig. 9 (c). The significant difference between La Niña and El Niño lasts from winter (DJF) to early summer (AMJ). The ozone concentration after El Niño is about 12 ppbv lower than after La Niña. This difference obtained from CLaMS simulations for the time period from 1979 to 2015 is slightly smaller than from MLS measurements for the time 10   period from 2004 to 2015.

4.3   In-mixing from SHADOZ

MLS measurements and CLaMS simulations above provide the ENSO-related differences in the horizontal distribution of ozone. The vertical influence of ENSO anomalies on the ozone distribution near the tropopause can also be inferred from the ozonesonde data observed at the SHADOZ station Hilo, Hawaii [19.43° N, 155.04° W] (marked with a star in Fig. 2, Fig. 7, 15   Fig. 8, and Fig. 9) from 1998 to 2015. Hilo is located in the central Pacific at the edge of the climatological position of the anticyclone in winter (see Fig. 2). The air over Hilo is strongly affected by the meridional disruption of the subtropical jet from winter (DJF) to early summer (AMJ) following La Niña winters, while it is within the tropics following El Niño winters.

The SHADOZ ozonesonde data are used to investigate the vertical distribution of the ENSO-related anomalies. The resolution of the ozone profiles is not the same for the whole period, so the data is degraded to the vertical resolution of 200 m for 20   all the years to calculate the statistical ozone profiles. The seasonal mean profiles following La Niña and El Niño winters are calculated for ENSO composites introduced in section 2. Fig. 10 shows the variation of ozone with altitude over Hilo from winter (DJF) to summer (JJA) following ENSO.

The mean ozone profiles following El Niño show a common vertical "S" shape structure for all the seasons, with the lowest value near the surface, a maximum near 6 km, a minimum near 12 km, and a subsequent in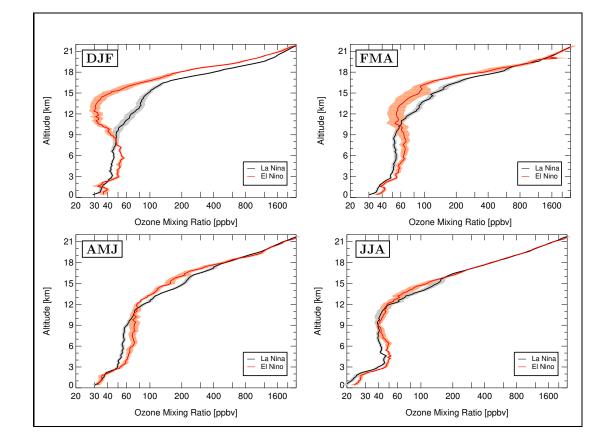crease toward stratospheric values. 25   However, the mean ozone profiles from La Niña do not exhibit this structure except for JJA. The low ozone concentrations of ≈ 30-40 ppbv at altitude of ≈ 12-14 km after El Niño are located at the level of main convective out flow and are therefore caused by uplift of tropospheric air by convection (Folkins et al., 2002; Thompson et al., 2012).

On the other hand, the ozone profiles after La Niña do not show an "S" shape. Fig. 10 shows that the ozone concentration in the middle troposphere following La Niña is lower than after El Niño, which will be discussed below. In addition, the ozone 30   concentration in the UTLS from DJF to AMJ following La Niña is higher than after El Niño. On average, the ozone concentration for La Niña is about 110 ppbv higher than for El Niño from 9 km to 21 km in DJF (top left). The ozone concentration difference between La Niña and El Niño during FMA (top right) becomes smaller than during DJF, when the mean difference is about 54 ppbv in the layer from 10 km to 20 km. The mean concentration of ozone following La Niña is higher than following El Niño from 11 km to 18 km during AMJ (bottom left), the difference is about 28 ppbv. There is no clear difference between

Figure 10. Ozonesonde measurements from SHADOZ in Hilo, Hawaii [19.43° N, 155.04° W] during 1998-2015. Black and red lines represent the seasonal mean profiles for La Niña and El Niño, respectively. The shade indicates the standard deviation of the mean. The location of the data used here is marked (star) in Fig. 2, Fig. 7, Fig. 8, and Fig. 9.

the two composites in the UTLS region during JJA (bottom right). The results from SHADOZ indicate that the air masses are more affected by in-mixing following La Niña years, and the strong meridional disruption of the subtropical jet and in-mixing phenomenon after La Niña impact the air masses not only at 380 K ($\approx$ 15 km) but also throughout the UTLS region. Especially in winter, ENSO anomalies have the strongest influence on ozone profile (from 9 km to 21 km). The influence lasts from winter

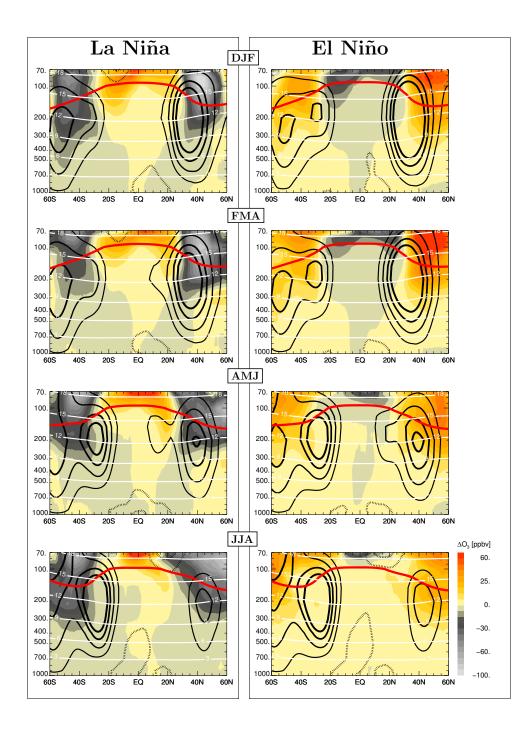5   (DJF) to early summer (AMJ), but vanishes during summer (JJA).

Note that the ozone after El Niño is higher than after La Niña in the middle troposphere (around 3-9 km) from SHADOZ data (Fig. 10). The zonal mean ozone anomalies in the west and central Pacific are calculated to understand the potential influence from ENSO. Fig. 11 shows seasonal results of zonal mean (120° E - 120° W) ozone anomalies after La Niña and El Niño from the surface to 70 hPa. The largest influence of ENSO on ozone occurs in the lower stratosphere, but the influence extends even

10   downward into the middle troposphere. In DJF and FMA following El Niño, the figure indicates that the ozone in the tropics

16

Figure 11. Zonally averaged ozone anomalies in west and central Pacific [120° E, 120° W] from DJF to JJA based on CLaMS simulations covering 1979-2015. The solid and dashed lines are the zonal means of the westerlies (10, 17, 24, and 30 m/s) and easterlies (−5, −10, and −20 m/s), respectively. Red lines represent θ=380 K level. White lines represent GPH (km).

shows a negative anomaly from the surface to the tropopause, whereas the ozone in the subtropics shows a positive anomaly behind subtropical jet. However, it shows an opposite pattern following La Niña. This manifests that the enhanced upwelling in the tropics in DJF and FMA following El Niño can bring ozone poor air from the surface to the high altitude above the tropopause. Likewise, the enhanced downwelling polewards of the subtropical jets (black lines in Fig. 11) following El Niño
5   can transport ozone rich air from the stratosphere to the middle troposphere. The higher ozone in the middle troposphere in Hilo during DJF and FMA following El Niño may be partially related to the isentropic transport of ozone-rich air from the stratosphere. The stratospheric influence on the subtropical middle troposphere, affecting the "S" shape of ozone profiles, was suggested by Pan et al. (2006); Hayashi et al. (2008); Konopka and Pan (2012); Neu et al. (2014). The difference becomes small in AMJ, and it disappears in JJA.

10   ## 5   Discussion

Inspired by the work of Chowdary et al. (2016) about the impact of no-decay El Niño on rainfall, El Niño episodes which last until the next winter are selected (1987 and 1992) and the influence on the atmospheric circulations and ozone distributions was investigated (details are omitted). The SF and VP distributions show strongest anomalies during these three years compared to all El Niño years. In particular, the ASM anticyclone is even weaker and the Hadley circulation is stronger during these periods.
15   Accordingly, the ozone concentrations in the tropics show weak intrusions from the subtropics during summer. This indicates that if El Niño does not decay until the following summer, the influence of El Niño on the ASM anticyclone and ozone will last longer.

   Neu et al. (2014) found that the superposition of El Niño and easterly QBO phase increases ozone flux from the stratosphere into the troposphere, resulting in enhanced tropospheric ozone values in mid-latitudes. In particular, increased convection over
20   the central/eastern Pacific results in a negative zonal mean ozone anomaly in the tropical upper troposphere. The opposite effect occurs for the combination of La Niña and westerly QBO phase. Here, we also check the influence of QBO on the results. Table 1 shows that La Niña winters are almost equally affected by westerly and easterly QBO phases, while during El Niño the westerly QBO phase occurs more often. To remove the potential influence of the QBO phase, the results from 4 years of westerly QBO (1997/1998 and 2006/2007) are excluded. The change of ozone concentration at 380 K caused by ENSO is
25   around 3% based on CLaMS simulations from winter to summer, the westerly phase causes slightly higher ozone concentration than easterly in the tropical upper troposphere. The change is less than 5% from SHADOZ data, and the westerly phase also causes slightly higher ozone in the UTLS region in Hilo. This indicates that our results about the ENSO effects are robust.

6   Conclusions

ENSO typically shows the strongest signal in winter, but it can affect the atmosphere until the next early summer. Here we try
30   to understand the influence of ENSO on the UTLS from a dynamical and atmospheric composition perspective. SF and VP are introduced to quantify the influence of ENSO on the atmosphere from a dynamical perspective. SF and VP represent the

Atmospheric
Chemistry
and Physics
Discussions

divergence free and rotation free part of the horizontal wind field, respectively. The results show that the subtropical jets after El Niño winters are more zonally symmetric. Furthermore, the meridional disruption of the subtropical jets during El Niño is weaker compared to La Niña winters. The anticyclonic circulations in the tropics following El Niño is weaker than following La Niña. The strength of the ASM anticyclone after El Niño is slightly weaker than after La Niña in early summer, and the

5 onset date after El Niño years is about half a month later than after La Niña years. VP after El Niño is weaker than after La Niña from winter until early summer because of the weaker Walker circulation after El Niño years. The Hadley circulation after El Niño is much stronger than after La Niña from winter to spring.

The anomalies of the atmospheric circulation caused by ENSO also affect the distribution of atmospheric composition. MLS satellite measurements (2004-2015) and CLaMS simulations (1979-2015) are used to analyse the horizontal influence

10 of ENSO on the ozone distribution. The results from CLaMS simulations show similar patterns as MLS measurements. They both manifest that ozone patterns after La Niña winters and springs show in-mixing over the east and central Pacific, while the ozone patterns after El Niño winters and springs are more zonally symmetric. The in-mixing difference between La Niña and El Niño is striking during the onset of the ASM anticyclone. The intrusions from the high latitude stratosphere reach much deeper into the tropics for La Niña compared to El Niño. This indicates that the ozone anomaly lags the atmospheric circulation

15 anomaly in El Niño/La Niña winters by about 4 months. The weaker in-mixing and strong Hadley circulation during El Niño causes smaller ozone mixing ratio in the tropics compared to La Niña in the UTLS from winter to early summer.

Based on the ozonesonde data from SHADOZ (1998-2015) in Hilo, Hawaii, the vertical impact of ENSO on the ozone distribution is investigated. The common vertical "S" shape structure only exists in the ozone profiles following El Niño rather than La Niña from winter to early summer. The ozone concentration in the UTLS after El Niño is lower than after La Niña from

20 DJF to AMJ. The results demonstrate that the air masses over Hilo following La Niña encounter stronger in-mixing comparing to El Niño. This significantly changes the ozone profiles after La Niña years.

Author contributions. TEXT

Competing interests. TEXT

Disclaimer. TEXT

25   0.2

Atmospheric
Chemistry
and Physics
Discussions

References

Bannister, R. N., O'Neill, A., Gregory, A. R., and Nissen, K. M.: The role of the south-east Asian monsoon and other seasonal features in creating the 'tape-recorder' signal in the Unified Model, Q. J. R. Meteorol. Soc., 130, 1531–1554, 2004.

Bjerknes, J.: Atmospheric teleconnections from the equatorial Pacific, Monthly Weather Review, 97, 163–172, 1969.

5 Bjerknes, V.: Sur les relations entre l'ozone et les mouvements de la troposphère, Gerl. Beitr. Geophys., 24, 23, 1929.

Calvo, N., Garcia, R. R., Randel, W. J., and Marsh, D.: Dynamical mechanism for the increase in tropical upwelling in the lowermost tropical stratosphere during warm ENSO events, J. Atmos. Sci., 67, 2331–2340, https://doi.org/10.1175/2010JAS3433.1, 2010.

Chen, P.: Isentropic cross-tropopause mass exchange in the extratropics, J. Geophys. Res., 100, 16 661–16 673, 1995.

Chowdary, J. S., Harsha, H. S., Gnanaseelan, C., Srinivas, G., Parekh, A., Pillai, P., and Naidu, C. V.: Indian summer monsoon rainfall
10   variability in response to differences in the decay phase of El Niño, Climate Dynamics, https://doi.org/10.1007/s00382-016-3233-1, 2016.

Dee, D. P., Uppala, S. M., Simmons, A. J., Berrisford, P., Poli, P., Kobayashi, S., Andrae, U., Balmaseda, M. A., Balsamo, G., Bauer, P., Bechtold, P., Beljaars, A. C. M., van de Berg, L., Bidlot, J., Bormann, N., Delsol, C., Dragani, R., Fuentes, M., Geer, A. J., Haimberger, L., Healy, S. B., Hersbach, H., Holm, E. V., Isaksen, L., Kallberg, P., Koehler, M., Matricardi, M., McNally, A. P., Monge-Sanz, B. M., Morcrette, J.-J., Park, B.-K., Peubey, C., de Rosnay, P., Tavolato, C., Thepaut, J.-N., and Vitart, F.: The ERA-Interim reanalysis: configuration
15   and performance of the data assimilation system, Q. J. R. Meteorol. Soc., 137, 553–597, https://doi.org/10.1002/qj.828, 2011.

Dethof, A., O'Neill, A., Slingo, J. M., and Smit, H. G. J.: A mechanism for moistening the lower stratosphere involving the Asian summer monsoon, Q. J. R. Meteorol. Soc., 556, 1079–1106, 1999.

Dunkerton, T. J.: Evidence of meridional motion in the summer lower stratosphere adjacent to monsoon regions, J. Geophys. Res., 100, 16,675–16,688, 1995.

20 Evans, J. L. and Allan, R. J.: El Nino/southern oscillation modification to the structure of the monsoon and tropical cyclone activity in the Australasian region, International Journal of Climatology, 12, 611–623, 1992.

Folkins, I., Braun, C., Thompson, A. M., and Witte, J.: Tropical ozone as an indicator of deep convection, Journal of Geophysical Research: Atmospheres, 107, ACH 13–1–ACH 13–10, https://doi.org/10.1029/2001JD001178, http://dx.doi.org/10.1029/2001JD001178, 2002.

Fu, R., Hu, Y., Wright, J. S., Jiang, J. H., Dickinson, R. E., Chen, M., Filipiak, M., Read, W. G., Waters, J. W., and Wu, D. L.: Short
25   circuit of water vapor and polluted air to the global stratosphere by convective transport over Tibetian Plateau, Proc. Nat. Acad. Sci., 103, 5664–5669, 2006.

Fueglistaler, S., Bonazzola, M., Haynes, P. H., and Peter, T.: Stratospheric water vapor predicted from the Lagrangian temperature history of air entering the stratosphere in the tropics, J. Geophys. Res., 110, D08107, https://doi.org/10.1029/2004JD005516, 2005.

Garfinkel, C. I., Hurwitz Margaret, M., Oman Luke, D., and Waugh, D. W.: Contrasting Effects of Central Pacific and Eastern Pacific El
30   Nino on stratospheric water vapor, grl, 40, 4115–4120, https://doi.org/10.1002/grl.50677, 2013.

Gettelman, A., Hoor, P., Pan, L. L., Randel, W. J., Hegglin, M. I., and Birner, T.: The extratropical upper troposphere and lower stratosphere, Rev. Geophys., 49, RG3003, https://doi.org/10.1029/2011RG000355, 2011.

Gill, A. E.: Some simple solutions for heat-induced tropical circulation, Q. J. R. Meteorol. Soc., 106, 447–462, 1980.

Hayashi, H., Kita, K., and Taguchi, S.: Ozone-enhanced layers in the troposphere over the equatorial Pacific Ocean and the influence of
35   transport of midlatitude UT/LS air, Atmos. Chem. Phys., 8, 2609–2621, 2008.

Haynes, P. and Shuckburgh, E.: Effective diffusivity as a diagnostic of atmospheric transport, 2, Troposphere and lower stratosphere, J. Geophys. Res., 105, 22 795–22 810, 2000.

Highwood, E. J. and Hoskins, B. J.: The tropical tropopause, Q. J. R. Meteorol. Soc., 124, 1579 – 1604, 1998.

Holton, J. R., Haynes, P., McIntyre, M. E., Douglass, A. R., Rood, R. B., and Pfister, L.: Stratosphere-troposphere exchange, Rev. Geophys., 33, 403–439, 1995.

Jiang, Y. B., Froidevaux, L., Lambert, A., Livesey, N. J., Read, W. G., Waters, J. W., Bojkov, B., Leblanc, T., McDermid, I. S., Godin-
5   Beekmann, S., Filipiak, M. J., Harwood, R. S., Fuller, R. A., Daffer, W. H., Drouin, B. J., Cofield, R. E., Cuddy, D. T., Jarnot, R. F., Knosp, B. W., Perun, V. S., Schwartz, M. J., Snyder, W. V., Stek, P. C., Thurstans, R. P., Wagner, P. A., Allaart, M., Andersen, S. B., Bodeker, G., Calpini, B., Claude, H., Coetzee, G., Davies, J., De Backer, H., Dier, H., Fujiwara, M., Johnson, B., Kelder, H., Leme, N. P., König-Langlo, G., Kyro, E., Laneve, G., Fook, L. S., Merrill, J., Morris, G., Newchurch, M., Oltmans, S., Parrondos, M. C., Posny, F., Schmidlin, F., Skrivankova, P., Stubi, R., Tarasick, D., Thompson, A., Thouret, V., Viatte, P., Vömel, H., von Der Gathen, P., Yela, M.,
10 and Zablocki, G.: Validation of Aura Microwave Limb Sounder Ozone by ozonesonde and lidar measurements, Journal of Geophysical Research: Atmospheres, 112, 2007.

Ju, J. and Slingo, J.: The Asian summer monsoon and ENSO, Quarterly Journal of the Royal Meteorological Society, 121, 1133–1168, 1995.

Kawamura, R.: A Possible Mechanism of the Asian Summer Monsoon-ENSO Coupling, Journal of the Meteorological Society of Japan. Ser. II, 76, 1009–1027, 1998.

15 Konopka, P. and Pan, L. L.: On the mixing-driven formation of the Extratropical Transition Layer (ExTL), J. Geophys. Res., 117, D18301, https://doi.org/10.1029/2012JD017876, 2012.

Konopka, P., Steinhorst, H.-M., Grooß, J.-U., Günther, G., Müller, R., Elkins, J. W., Jost, H.-J., Richard, E., Schmidt, U., Toon, G., and McKenna, D. S.: Mixing and Ozone Loss in the 1999-2000 Arctic Vortex: Simulations with the 3-dimensional Chemical Lagrangian Model of the Stratosphere (CLaMS), J. Geophys. Res., 109, D02315, https://doi.org/10.1029/2003JD003792, 2004.

20 Konopka, P., Grooß, J.-U., Günther, G., Ploeger, F., Pommrich, R., Müller, R., and Livesey, N.: Annual cycle of ozone at and above the tropical tropopause: observations versus simulations with the Chemical Lagrangian Model of the Stratosphere (CLaMS), Atmos. Chem. Phys., 10, 121–132, https://doi.org/10.5194/acp-10-121-2010, http://www.atmos-chem-phys.net/10/121/2010/, 2010.

Konopka, P., Ploeger, F., Tao, M., and Riese, M.: Zonally resolved impact of ENSO on the stratospheric circulation and water vapor entry values, Journal of Geophysical Research: Atmospheres, 121, 11,486–11,501, 2016.

25 Krüger, K., Tegtmeier, S., and Rex, M.: Long-term climatology of air mass transport through the Tropical Tropopause Layer (TTL) during NH winter, Atmos. Chem. Phys., 8, 813–823, 2008.

Kunze, M., Braesicke, P., Langematz, U., and Stiller, G.: Interannual variability of the boreal summer tropical UTLS in observations and CCMVal-2 simulations, Atmospheric Chemistry and Physics, 16, 8695–8714, https://doi.org/10.5194/acp-16-8695-2016, https://www.atmos-chem-phys.net/16/8695/2016, 2016.

30 Liess, S. and Geller, M. A.: On the relationship between QBO and distribution of tropical deep convection, J. Geophys. Res., 117, D03108, https://doi.org/10.1029/2011JD016317, 2012.

Livesey, N. J., Read, W. G., Wagner, P. A., Froidevaux, L., Lambert, A., Manney, G. L., Valle, L. F. M., Pumphrey, H. C., Santee, M. L., Schwartz, M. J., Wang, S., Fuller, R. A., Jarnot, R. F., Knosp, B. W., and Martinez, E.: Version 4.2x Level 2 data quality and description document, 2017.

35 Matsuno, T.: Quasi-geostrophic motopns in the equatorial area, J. Meteorol. Soc. Jpn., 44, 25–42, 1966.

McKenna, D. S., Konopka, P., Grooß, J.-U., Günther, G., Müller, R., Spang, R., Offermann, D., and Orsolini, Y.: A new Chemical Lagrangian Model of the Stratosphere (CLaMS): 1. Formulation of advection and mixing, J. Geophys. Res., 107, 4309, https://doi.org/10.1029/2000JD000114, 2002.

Atmospheric
Chemistry
and Physics
Discussions

McPhaden, M. J.: Playing hide and seek with El Nino, Nature Climate Change, 5, 791–795, 2015.

McPhaden, M. J., Zebiak, S. E., and Glantz, M. H.: ENSO as an integrating concept in Earth science, Science, 314, 1740–1745, 2006.

Moron, V. and Gouirand, I.: Seasonal modulation of the El Niño–southern oscillation relationship with sea level pressure anomalies over the North Atlantic in October–March 1873–1996, International Journal of Climatology, 23, 143–155, https://doi.org/10.1002/joc.868, http://dx.doi.org/10.1002/joc.868, 2003.

Müller, S., Hoor, P., Bozem, H., Gute, E., Vogel, B., Zahn, A., Bönisch, H., Keber, T., Krämer, M., Rolf, C., Riese, M., Schlager, H., and Engel, A.: Impact of the Asian monsoon on the extratropical lower stratosphere: trace gas observations during TACTS over Europe 2012, Atmospheric Chemistry & Physics, 16, 10 573–10 589, https://doi.org/10.5194/acp-16-10573-2016, 2016.

Neu, J. L., Flury, T., Manney, G. L., Santee, M. L., Livesey, N. J., and Worden, J.: Tropospheric ozone variations governed by changes in stratospheric circulation, Nature Geosci, 7, 340–344, https://doi.org/10.1038/ngeo2138, 2014.

Pan, L. L., Konopka, P., and Browell, E. V.: Observations and model simulations of mixing near the extratropical tropopause, J. Geophys. Res., 111, D05106, https://doi.org/10.1029/2005JD006480, 2006.

Park, M., Randel, W. J., Gettelman, A., Massie, S. T., and Jiang, J. H.: Transport above the Asian summer monsoon anticyclone inferred from Aura Microwave Limb Sounder tracers, Journal of Geophysical Research: Atmospheres, 112, 2007.

Park, M., Randel, W. J., Emmons, L. K., Bernath, P. F., Walker, K. A., and Boone, C. D.: Chemical isolation in the Asian monsoon anticyclone observed in Atmospheric Chemistry Experiment (ACE-FTS) data, Atmos. Chem. Phys., 8, 757–764, 2008.

Philander, S., Holton, J., and Dmowska, R.: El Nino, La Nina, and the Southern Oscillation, vol. 46 of *International Geophysics*, Academic Press, https://books.google.de/books?id=9fwrkW_B1YYC, 1989.

Ploeger, F., Konopka, P., Müller, R., Fueglistaler, S., Schmidt, T., Manners, J. C., Grooß, J.-U., Günther, G., Forster, P. M., and Riese, M.: Horizontal transport affecting trace gas seasonality in the Tropical Tropopause Layer (TTL), J. Geophys. Res., 117, D09303, https://doi.org/10.1029/2011JD017267, warning: BibtexKey has changed!!, 2012.

Ploeger, F., Günther, G., Konopka, P., Fueglistaler, S., Müller, R., Hoppe, C., Kunz, A., Spang, R., Grooß, J.-U., and Riese, M.: Horizontal water vapor transport in the lower stratosphere from subtropics to high latitudes during boreal summer, J. Geophys. Res., 118, 8111–8127, https://doi.org/10.1002/jgrd.50636, 2013.

Ploeger, F., Riese, M., Haenel, F., P.Konopka, Müller, R., and Stiller, G.: Variability of stratospheric mean age of air and of the local effects of residual circulation and eddy mixing, J. Geophys. Res., 120, 716–733, https://doi.org/10.1002/2014JD022468, 2015.

Ploeger, F., Konopka, P., Walker, K., and Riese, M.: Quantifying pollution transport from the Asian monsoon anticyclone into the lower stratosphere, Atmos. Chem. Phys., 16, 7055–7066, https://doi.org/10.5194/acp-17-7055-2017, 2017.

Pommrich, R., Müller, R., Grooß, J.-U., Konopka, P., Ploeger, F., Vogel, B., Tao, M., Hoppe, C. M., Günther, G., Spelten, N., Hoffmann, L., Pumphrey, H.-C., Viciani, S., D'Amato, F., Volk, C. M., Hoor, P., Schlager, H., and Riese, M.: Tropical troposphere to stratosphere transport of carbon monoxide and long-lived trace species in the Chemical Lagrangian Model of the Stratosphere (CLaMS), Geoscientific Model Development, 7, 2895–2916, https://doi.org/10.5194/gmd-7-2895-2014, http://www.geosci-model-dev.net/7/2895/2014/, 2014.

Pumphrey, H. C., Glatthor, N., Bernath, P. F., Boone, C. D., Hannigan, J., Ortega, I., Livesey, N. J., and Read, W. G.: MLS measurements of stratospheric hydrogen cyanide during the 2015–16 El Niño event, Atmospheric Chemistry and Physics Discussions, 2017, 1–18, 2017.

Randel, W. J. and Park, M.: Deep convective influence on the Asian summer monsoon anticyclone and associated tracer variability observed with Atmospheric Infrared Sounder (AIRS), J. Geophys. Res., 111, D12314, https://doi.org/10.1029/2005JD006490, 2006.

Randel, W. J., Garcia, R. R., Calvo, N., and Marsh, D.: ENSO influence on zonal mean temperature and ozone in the tropical lower stratosphere, Geophys. Res. Lett., 36, L15822, https://doi.org/10.1029/2009GL039343, 2009.

Atmospheric
Chemistry
and Physics
Discussions

Randel, W. J., Park, M., Emmons, L., Kinnison, D., Bernath, P., Walker, K. A., Boone, C., and Pumphrey, H.: Asian Monsoon Transport of Pollution to the Stratosphere, Science, 328, 611–613, https://doi.org/10.1126/science.1182274, 2010.

Rolf, C., Vogel, B., Hoor, P., Afchine, A., Günther, G., Krämer, M., Müller, R., Müller, S., Spelten, N., and Riese, M.: Water vapor increase in the northern lower stratosphere by the Asian monsoon anticyclone observed during TACTS/ESMVal campaigns, Atmospheric Chemistry and Physics Discussions, 2017, 1–16, 2017.

5

Santee, M. L., Manney, G. L., Livesey, N. J., Froidevaux, L., Schwartz, M. J., and Read, W. G.: Trace gas evolution in the lowermost stratosphere from Aura Microwave Limb Sounder measurements, J. Geophys. Res., 116, 2011.

Santee, M. L., Manney, G. L., Livesey, N. J., Schwartz, M. J., Neu, J., and Read, W. G.: A comprehensive overview of the climatological composition of the Asian summer monsoon anticyclone based on 10 years of Aura Microwave Limb Sounder measurements, J. Geophys.

10 Res., 122, 2017.

Scaife, A. A., Butchart, N., Jackson, D. R., and Swinbank, R.: Can changes in ENSO activity help to explain increasing stratospheric water vapor?, Geophys. Res. Lett., 30, https://doi.org/10.1029/2003GL017591, 2003.

Tanaka, H. L., Ishizaki, N., and Kitoh, A.: Trend and interannual variability of Walker, monsoon and Hadley circulations defined by velocity potential in the upper troposphere, Tellus A, 56, 250–269, 2004.

15 Thompson, A. M., Witte, J. C., Smit, H. G. J., Oltmans, S. J., Johnson, B. J., Kirchhoff, V. W. J. H., and Schmidlin, F. J.: Southern Hemisphere Additional Ozonesondes (SHADOZ) 1998-2004 tropical ozone climatology: 3. Instrumentation, station-to-station variability, and evaluation with simulated flight profiles, J. Geophys. Res., 112, 1297–1300, https://doi.org/10.1029/2005JD007042, 2007.

Thompson, A. M., Miller, S. K., Tilmes, S., Kollonige, D. W., Witte, J. C., Oltmans, S. J., Johnson, B. J., Fujiwara, M., Schmidlin, F. J., Coetzee, G. J. R., Komala, N., Maata, M., bt Mohamad, M., Nguyo, J., Mutai, C., Ogino, S.-Y., Da Silva, F. R., Leme, N. M. P., Posny, F.,

20 Scheele, R., Selkirk, H. B., Shiotani, M., Stübi, R., Levrat, G., Calpini, B., Thouret, V., Tsuruta, H., Canossa, J. V., Vömel, H., Yonemura, S., Diaz, J. A., Tan Thanh, N. T., and Thuy Ha, H. T.: Southern Hemisphere Additional Ozonesondes (SHADOZ) ozone climatology (2005–2009): Tropospheric and tropical tropopause layer (TTL) profiles with comparisons to OMI-based ozone products, Journal of Geophysical Research: Atmospheres, 117, 2012.

Thouret, V., Cammas, J.-P., Sauvage, B., Athier, G., Zbinden, R., Nédélec, P., Simon, P., and Karcher, F.: Tropopause referenced ozone

25 climatology and inter-annual variability (1994–2003) from the MOZAIC programme, Atmospheric Chemistry and Physics, 6, 1033–1051, 2006.

Vogel, B., Günther, G., Müller, R., Grooß, J.-U., Afchine, A., Bozem, H., Hoor, P., Krämer, M., Müller, S., Riese, M., Rolf, C., Spelten, N., Stiller, G. P., Ungermann, J., and Zahn, A.: Long-range transport pathways of tropospheric source gases originating in Asia into the northern lower stratosphere during the Asian monsoon season 2012, Atmospheric Chemistry and Physics, 16, 15 301–15 325, 2016.

30 Walker, G. T.: Correlation in seasonal variations of weather. VIII: A preliminary study of world weather, 1923.

Wang, C. and Picaut, J.: Understanding ENSO physics - A review, in: Earth's Climate: The Ocean-Atmosphere Interaction, edited by Wang, C., Xie, S.-P., and Carton, J. A., vol. 147 of *Geophysical Monograph Series*, pp. 21–38, AGU, 2004.

Wang, H. J., Cunnold, D. M., Thomason, L. W., Zawodny, J. M., and Bodeker, G. E.: Assessment of SAGE version 6.1 ozone data quality, J. Geophys. Res., 105, 4691, https://doi.org/10.1029/2002JD002418, 2002.

35 Wang, X., Jiang, X., Yang, S., and Li, Y.: Different impacts of the two types of El Niño on Asian summer monsoon onset, Environmental Research Letters, 8, 044 053, http://stacks.iop.org/1748-9326/8/i=4/a=044053, 2013.

Waugh, D. W. and Polvani, L. M.: Climatology of intrusions into the tropical upper troposphere, Geophys. Res. Lett., 27, 3857–3860, 2000.

Wolter, K.: The Southern Oscillation in surface circulation and climate over the tropical Atlantic, Eastern Pacific, and Indian Oceans as captured by cluster analysis., J. Climate Appl. Meteor., 26, 540–558, 1987.

Wright, J. S., Fu, R., Fueglistaler, S., Liu, Y. S., and Zhang, Y.: The influence of summertime convection over Southeast Asia on water vapor in the tropical stratosphere, J. Geophys. Res., 116, D12302, https://doi.org/10.1029/2010JD015416, 2011.

Yan, X., Wright, J. S., Zheng, X., Livesey, N. J., Vömel, H., and Zhou, X.: Validation of Aura MLS retrievals of temperature, water vapour and ozone in the upper troposphere and lower–middle stratosphere over the Tibetan Plateau during boreal summer, Atmospheric Measurement Techniques, 9, 3547–3566, https://doi.org/10.5194/amt-9-3547-2016, https://www.atmos-meas-tech.net/9/3547/2016/, 2016.

Zhang, Z. and Krishnamurti, T. N.: A Generalization of Gill's Heat-Induced Tropical Circulation, J. Atmos. Sci., 53, 1045–1052, 2006.

Ziemke, J. R., Douglass, A. R., Oman, L. D., Strahan, S. E., and Duncan, B. N.: Tropospheric ozone variability in the tropics from ENSO to MJO and shorter timescales, Atmospheric Chemistry and Physics, 15, 8037–8049, 2015.